The Effect of Aerated Oil Considering Live Oil Surface Tension on High-Speed Journal Bearing

Sang Myung Chun[†]

Kookmin University, Graduate School of Automotive Engineering, 861-1 Chungnung-dong, Sungbuk-gu, Seoul, 136-702, Korea

Abstract: The influence of aerated oil on high-speed journal bearing is examined by classical thermohydrodynamic lubrication theory coupled with analytical models for viscosity and density of air-oil mixture in fluid-film bearing. Convection to the walls and mixing with supply oil and re-circulating oil are considered. The live oil surface tension is considered as functions of temperature, API gravity and air volume ratio. With changing eccentricity ratio, it is investigated the effects of air bubbles on the performance of a high-speed plain journal bearing. Just at the moderate eccentricity ratios, even if the involved aeration levels are not so severe and the entrained air bubble sizes are not so small, it is found that the bearing load and friction force may be changed so visibly for the high speed bearing operation.

Key words: Aerated oil, flow mixing, eccentricity ratio, convective conditions on the walls, high-speed journal bearing, turbulent reynolds and energy equations; live oil surface tension

Introduction

The onset of turbulence in connection with bearings had not become evident until Wilcock (1) discovered its effects on bearing performance by a series of experiments. The basic turbulent lubrication theory had been developed by several researchers (2-7). The most of researchers handled lubricant as incompressible pure oil.

Meanwhile, a simple empirical viscosity relationship for gas-liquid mixture was found by Hayward (8) using a parameter of air-oil volume ratio.

Smith (9) assumed that the aerated oil was isoviscous, but accounted for the effects of bubble surface tension on density. He found that the load capacity was virtually unaffected by aeration rate.

Abdel-Latif *et al.* (10) considered circular pad thrust bearings. They used simply density and viscosity models, extended to account for temperature effects, and found that aeration rate had little effect on load capacity.

Chamniprasart *et al.* (11) derived an extended Reynold's equation to account for the fact that aerated oil is non Newtonian. They used a viscosity model similar to Haywards [8]. They found that the bearing pressure increases initially with aeration rate, but that the trend is reversed at very high aeration rates when the lubricant starts to behave as a gas.

A first effort to derive an analytical model for aerated oil viscosity is presented in Nikolajsen (12). This model predicts an increase in viscosity with increasing aeration level due to the surface tension of the entrained air bubbles. The predicted viscosity increase is confirmed by the experimental findings of

Hayward (8). A corresponding density model for aerated oil is also presented in Nikolajsen (12). Nikolajsen applied the mixture theory for aerated oil to one-dimensional Reynolds equation by assuming that the bearing is long (13). However, he did not consider energy equation.

The problem of predicting bearing performance when lubricating with bubbly oil could be attacked in two different ways. One could attempt to derive an effective viscosity and density like Nikolajsen (12) for bubbly oil which, when substituted into the classical Reynolds equation, predicts bearing performance correctly. Another method employs the viscosity of the oil itself but changes the Reynolds equation to accommodate a mixture lubricant like Chamniprasart *et al.* (11).

In this paper, the Nikolajsen's viscosity and density models (12) are used together with classical Reynolds equation and energy equation to investigate and predict numerically the effects of oil aeration on the performance of a high-speed plane journal bearing with an axial groove under the various conditions of eccentricity ratio.

Also, the convective conditions on the walls, the contraction ratio at cavitation region, and the mixing between re-circulating oil and inlet oil are included.

Governing Equations

The Reynold's equation (2,3) for a steadily loaded journal bearing for finite width may be written as

$$\frac{\partial}{\partial x}\left(\frac{\rho h^3}{\mu}G_x\frac{\partial \bar{p}_g}{\partial x}\right) + \frac{\partial}{\partial z}\left(\frac{\rho h^3}{\mu}G_z\frac{\partial \bar{p}_g}{\partial z}\right) = \frac{U}{2}\frac{\partial(\rho h)}{\partial x} \tag{1}$$

[†]Corresponding author; Tel: 82-2-910-4806, Fax: 82-2-910-4836
E-mail: smchun@kmu.kookmin.ac.kr

The appropriate values G_x of G_z and are given by the following (4,5) in the range $1{,}000{\leq}Re{\leq}30{,}000$.

$$G_x = \frac{1}{12 + 0.0136\left(\frac{hU}{v}\right)^{0.9}}$$ (2)

$$G_z = \frac{1}{12 + 0.0043\left(\frac{hU}{v}\right)^{0.96}}$$ (3)

The steady state two dimensional energy equation (5-7) with heat transfer boundary conditions at the bearing walls may be derived under turbulence conditions as

$$\rho\left\{\left(\frac{Uh}{2} - \frac{h^3}{\mu}G_x\frac{\partial \bar{p}_g}{\partial x}\right)\frac{\partial(C_p\bar{T})}{\partial x} - \frac{h^3}{\mu}G_z\frac{\partial \bar{p}_g}{\partial z}\frac{\partial(C_p\bar{T})}{\partial z}\right\} =$$

$$\tau_c U + \frac{h^3}{\mu}\left\{G_x\left(\frac{\partial \bar{p}_g}{\partial x}\right)^2 + G_z\left(\frac{\partial \bar{p}_g}{\partial z}\right)^2\right\} - (q_{sT} + q_{bT})$$ (4)

where,

$$q_{sT} = H_{sT}(\bar{T} - T_s)$$

$$q_{bT} = H_{bT}(\bar{T} - T_b)$$

The values of H_s and H_b (14) are chosen as shown in Table 3. In the range $1{,}000{\leq}Re{\leq}30{,}000$, appropriate values of

$$\bar{\tau}_c\left(= \tau_c/\frac{\mu U}{h}\right) \text{ are given by the following (4,5):}$$

$$\bar{\tau}_c = 1 + 0.0012\left(\frac{\rho U h}{\mu}\right)^{0.94}$$ (5)

The density (kg/m³) and kinematic viscosity (cst) of engine lubricant (15) can be expressed by equation [6] and equation [7] with constants, aa, bb and cc which vary depending on the kinds of the oil:

$$\rho_{oil} = 0.0361(aa - 0.000354T_f) \cdot 27680,$$ (6)

$$v_{oil} = \frac{\mu_{oil}}{\rho_{oil}} = 10^{10^{(bb - cc\log_{10}(T_r))}} - 0.6.$$ (7)

where T_f and T_r represent the Fahrenheit temperature and Rankin temperature, respectively. The values of aa, bb, and cc are 0.9070, 9.8500 and 3.5180, respectively, for a current oil. And C_p is the specific heat (J/kg. °C) of oil (16) that may be correlated with Celsius temperature T_c as equation [8].

$$C_p = 1796 + \frac{691}{160}T_c$$ (8)

The density (kg/m³) and dynamic viscosity (Pa·s) of aerated oil is derived in (12) as shown below. Non-dimensional density can be described as

$$\bar{p} = \frac{\rho}{\rho_{oil}} = \frac{(1 + \delta)\left(\bar{P}_{oil} + 2\frac{\bar{\sigma}}{r}\right)}{\delta + \bar{P}_{oil} + 2\frac{\bar{\sigma}}{r}},$$ (9)

where,

$$\delta = \frac{m_{air}}{m_{oil}} = \frac{(\bar{P}_{oil})_{in} + 2\bar{\sigma}/\bar{r}_{in}}{\frac{3}{4\pi}\left(\frac{\bar{r}_{in}}{\bar{d}_{in}}\right) - 1}, \quad \bar{\sigma} = \sigma/(\rho_{oil}\bar{R}T_c),$$

$$\bar{p} = p/(\rho_{oil}\bar{R}T).$$

$\bar{r}$ is the real root between 0 and $\bar{r}_{in}$ of the polynomial equation

$$\bar{p}_{oil}\bar{r}^{-3} + 2\bar{\sigma}\bar{r}^{-2} - [(\bar{p}_{oil})_{in} + 2\bar{\sigma}/\bar{r}_{in}]\bar{r}_{in}^{-3} = 0.$$

And c is the reference clearance, T is the absolute oil temperature, ρ_{oil} is the density of pure oil, σ is the surface tension of a bubble (N/m), and R is the gas constant (J/kg K). The surface tension (N/m) of a bubble in gas-oil mixture can be expressed as (17):

$$\sigma = \sigma_p[1/(1+0.02549V^{1.0157})]^* 10^{-3}$$ (10)

Here σ_p, $AT(38.085-0.259API)$, $AT = 1.11591-0.00305T_c$, $API = 141.5/SpGr-131.5$, $SpGr = SpGr60-0.00035(T_f- 60.)$, SpGr60 is a specific gravity of oil at 60 degree Fahrenheit.

Non-dimensional viscosity (12) can be expressed as:

$$\bar{\mu} = \frac{\mu}{\mu_{oil}} = \bar{\mu}_1 + \bar{\mu}_2$$ (11)

where $\bar{\mu}_1 = \frac{\mu_1}{\mu_{oil}} = \frac{\bar{p}}{1+\delta}$, $\bar{\mu}_2 = \frac{\mu}{\mu_{oil}} = \Gamma\bar{h}_{in}^{-3/2}\bar{r}/\sqrt{\bar{h}}$,

$$\Gamma = \frac{\pi^2\sigma}{\sqrt{2}\mu_{oil}U\bar{r}_{in}^{-3}}\left[\frac{r_{in}}{d_{in}}\right]^3, \quad \bar{h} = \frac{h}{c}, \quad \bar{d} = \frac{d}{c}$$

And U is the bearing surface speed. d is the distance between bubbles. $\bar{\mu}_1$ represents the viscosity reduction due to the near-zero air viscosity within the bubbles. $\bar{\mu}_2$ represents the viscosity increase due to bubble surface tension. $r_{in}/\bar{d}_{in}$ represents oil aeration level illustrated in Fig. 1.

Air volume ratio can be expressed as equation [12] in geometrical aspects of oil aeration level.

$$V = \frac{4\pi}{3A^3}$$ (12)

where $A = 1/[2(\bar{r}/\bar{d})_{in}] + 1$.

Note that the density of equation [9] and the viscosity of equation [11] are functions of the absolute oil film pressure $\bar{p}$, whereas Reynold's equation [1] and energy equation [4] are written as usual in terms of the gage pressure $\bar{p}_g$.
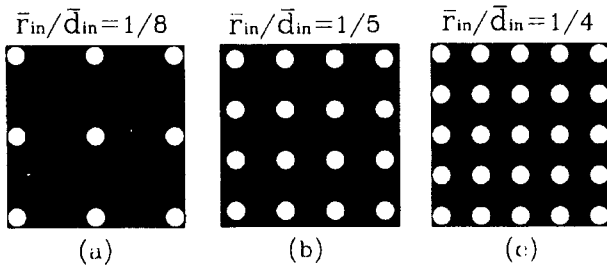
$\bar{r}_{in}/\bar{d}_{in} = 1/8$ $\bar{r}_{in}/\bar{d}_{in} = 1/5$ $\bar{r}_{in}/\bar{d}_{in} = 1/4$

(a)   (b)   (c)

Fig. 1. Oil aeration levels.

Film thickness, h, can be defined by the expression using bearing coordinates (18):

$$h = c(1 + \varepsilon \cos(\theta - \varphi)) \tag{13}$$

Boundary Conditions

The gage pressure at the ends of a finite length bearing is taken to be equal to the ambient pressure that is defined as being zero. Thus

$$\bar{p}_{z = \pm L/2} = 0 \tag{14}$$

At the point of film rupture, the pressure boundary conditions are

$$\bar{p} = \frac{\partial \bar{p}}{\partial \theta} = 0 \text{ at } \theta = \theta^* \tag{15}$$

At the ends of bearing, it is reasonable to assume that no heat will be transferred to the surrounding in the axial direction at the ends of the bearing. That is, the oil temperature having come out to the surrounding is assumed the same as of that at the end of the bearing, so

$$q_{z = \pm L/2} = 0. \tag{16}$$

For oil mixing condition, at the groove, the oil temperature is assumed as the mixing temperature between the re-circulating oil and inlet oil as shown on Fig. 2. The detailed expression is defined as

$$T_{mix} = \frac{(Q_{in} - Q_L)T_{in} + L_c Q_{rec} T_{rec}}{(Q_{in} - Q_L) + L_c Q_{rec}}. \tag{17}$$

where L_c is contraction ratio (19) of oil film that defined as

$$L_c(\theta) = \frac{\int_{-L/2}^{L/2} \int_0^{h(\theta^*, z)} u(\theta^*, z) dy dz}{\int_{-L/2}^{L/2} \int_0^{h(\theta, z)} u(\theta, z) dy dz}. \tag{18}$$

This ratio is the effective wetted width of the bush in the cavitating region. Then the heat transfer coefficient to the bush, adjusted for the reduction of wetting area in the cavitating region by the contraction ratio, becomes

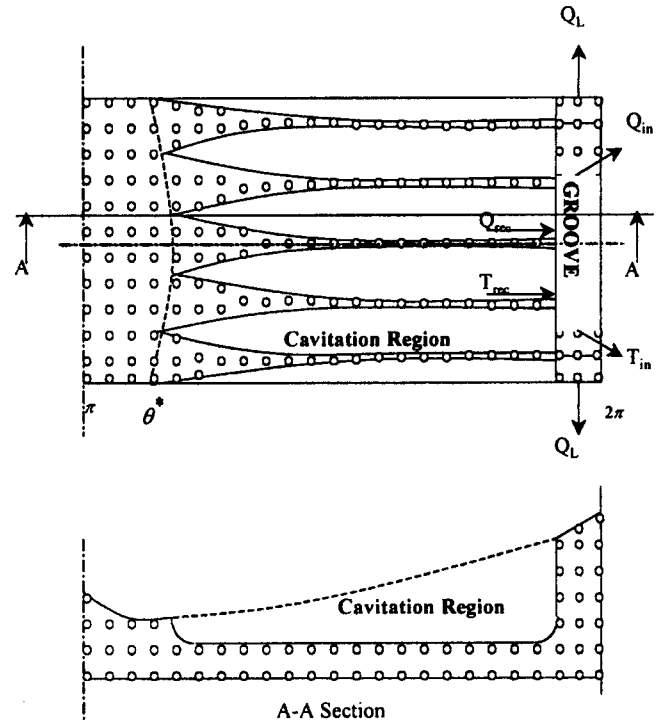$$H_b = L_c H^*_{bo} + (1 - L_c) H_{bg}. \tag{19}$$

Fig. 2. Diagram of lubricant flow, with Q_{in} the inlet oil flow rate, Q_{rec} the re-circulating flow rate and Q_L the side oil flow rate going through groove land. ϑ^* is the angle of the beginning of the cavitation region.

where H^*_{bo} is the mixed heat transfer coefficient of aerated oil that is adjusted with air volume ratio (V). It can be expressed that $H^*_{bo} = H_{bo}(1 - V) + H_{bg} V$.

The cavitation model of this study is shown on Fig. 2 that shows several oil strips and oil covering over shaft as usual. The size of air bubble varies depending on pressure. Meanwhile, the distribution of air inside oil is viewed as uniform. It is assumed that the air bubbles still exist uniformly even inside oil strips. The temperature distribution at air in cavitation region is the same as the temperature of aerated oil. The gage pressure in cavitation region is zero as mentioned as the boundary condition.

Therefore, synthetically speaking, for the turbulence treatment of fluid inside bearing, the mixed oil is treated as a sort of virtual oil whose physical properties appear the mixed viscosity, the mixed density and the specific heat of oil itself. However, the heat transfer to the bearing walls is handled separately from both oil and gas.

Calculation of Parameters

The non-dimensional load parameter components $\bar{W}_c$ and $\bar{W}_P$, parallel and normal to the line of centers respectively, are given by:

$$\bar{W}_c = \frac{W_c}{LD}\left(\frac{c}{R}\right)^2\left(\frac{L}{D}\right)/\mu_0 N = -\frac{1}{4}\int_0^{2\pi}\int_{-L/D}^{L/D} \bar{p}\cos\theta d\bar{z}d\theta \tag{20a}$$

and

$$\overline{W}_p = \frac{W_p}{LD}\left(\frac{c}{R}\right)^2\left(\frac{L}{D}\right)/\mu_0 N = \frac{1}{4}\int_0^{2\pi}\int_{-L/D}^{L/D}\bar{p}\sin\theta d\bar{z}d\theta \quad (20b)$$

Note that the total load parameter, $\overline{W}$, will be

$$\overline{W} = \sqrt{(\overline{W}_c^2 + \overline{W}_c^2)}. \quad (20c)$$

For turbulent flow, the non-dimensional form of total friction force can be expressed as follows

$$\overline{F}_t = \frac{F_t}{LD}\left(\frac{c}{R}\right)\left(\frac{L}{D}\right)/\mu_0 N$$

$$= \frac{1}{4}\int_0^{2\pi}\int_{-L/D}^{L/D}\left(G_x\frac{H}{2}\frac{\partial\overline{P}}{\partial\theta} + \overline{\tau}_c\bar{\mu}\frac{2\pi}{H}\right)d\bar{z}d\theta$$

The frictional torque is equal to friction force multiplied by the radius of a bearing and the frictional power loss is friction force multiplied by the velocity of the bearing shaft.

Computation

The turbulent Reynolds and the energy equations with turbulent similarity parameters have been solved by finite difference method using relaxation factors. Here, over-relaxation factors are used for solving Reynolds equation and under-relaxation factors for solving energy equation. The central finite difference technique is applied to the non-dimensional Reynolds equation. The backward difference scheme in the circumferential direction, and backward and forward difference schemes in the axial direction are used to the non-dimensional energy equation. In this study, the grid used comprises 43 × 15 nodes.

In order to create finite difference model in the cavitation region, the total width of oil strips are divided by total numbers of meshes in z-direction, then the small oil strip is allocated at each node. So it is assumed that the oil strip exits at each node.

With the pressure and temperature distributions thus specified, the load and friction parameters can then be computed from equation [20c] and [21].

Results and Discussions

In this study, the analysis results of bubbly lubrication are performed under high-speed operation considering the convective conditions on the walls, the contraction ratio at cavitation region, and the mixing between re-circulating oil and inlet oil.

The bearing geometry parameters and the lubricant properties used, are summarized in Table 1. A bearing with one axial groove has been examined. The basic algorithm of a numerical model used for this study had been verified by Chun (20).

The model of Chamniprasart et al (11) is based on the idea

Table 1. Journal bearing operating conditions

Bearing Diameter	D = 73.6 mm
L/D Ratio	0.5
c/R Ratio	0.0039837
Eccentricity Ratio	ε = 0.1~0.8
Rotational Speed	N = 40,000 rpm
Lubricant Viscosity at 40 °C	μ_0 = 0.0206 Pa · s
Lubricant Density at 40 °C	ρ_0 = 869.53 Kg/m^3
Lubricant Specific Heat at 40 °C	C_0 = 1968.75 J/kg °C
Convective Heat Transfer Coefficient of Lubricant to Bush	H_{boT} = 7700 W/m^2 °C
Convective Heat Transfer Coefficient of Gas(Air) to Bush	H_{bgT} = 2400 W/m^2 °C
Convective Heat Transfer Coefficient of Lubricant to Shaft	H_{sT} = 7700 W/m^2 °C
Bush and Shaft Temperature	$T_{b,s}$ = 45 °C
Inlet Lubricant Temperature	T_{in} = 40 °C
Inlet Lubricant Pressure(gage)	P_{in} = 0.7×10^5 Pa
Axial Groove Width	17.1 ° (2 grids size)

of mixture homogeneity. If the ratio r/c is sufficiently small, the roughness of scale of observation permits viewing the mixture as homogeneous. But the allowable upper limit of this ratio is not known. With the parameters of D = 38.1 mm, L/D = 1.3, c/R = 0.005984, ε = 0.4 and N = 4,000 rpm, they concluded that bubble size has only small effect on bearing pressure when changing from $\bar{r}_{in}$ = 0.1 to 0.45. But changing the air volume fraction of the bath from V = 0.02 to 0.2, the lubricant pressure changes significantly.

Nikolajsen (13) applied his air-oil mixed model of density and viscosity on a long bearing with D = 100 mm, c/R = 0.001 and N = 3600 rpm under the condition of bubble radius below $\bar{r}_{in}$ = 1/20 (0.05). As $\bar{r}_{in}$ is 1/20, the bearing loads are nearly not changed under the conditions of the aeration level, $\bar{r}_{in}/\bar{d}_{in}$, from 1/8 to 1/2. However, if $\bar{r}_{in}$ is 1/200 (0.005), it is shown that the bearing loads increase with increasing aeration level.

In this study, under high speed operating condition, the aeration levels, $\bar{r}_{in}/\bar{d}_{in}$, investigated are 1/8, 1/5, 1/4 and 1/3.5. These values are corresponding to the air volume ratios, V, of 0.0335, 0.0977, 0.1551 and 0.2383 respectively. And the sizes of air bubble, $\bar{r}_{in}$ (r_{in}) examined are 1/20 (7.3 μm), 1/15 (9.8 μm), 1/10 (14.7 μm) and 1/7 (20.9 μm). As $\bar{r}_{in}/\bar{d}_{in}$ increases, it is not able to handle the case of small air bubble size due to difficulties in numerical calculation. Therefore, the handled aeration levels are not so severe and the considered air bubble sizes are not so small as compared with those used by the previous studies (11, 13).

Under the bearing operating conditions of Table 1, the non-dimensional load and friction are shown in Fig. 3, Fig. 4, Fig. 5 and Fig. 6 for $(r/c)_{in}$ = 1/20, 1/15, 1/10 and 1/7 respectively. Generally, the non-dimensional load and friction increase with
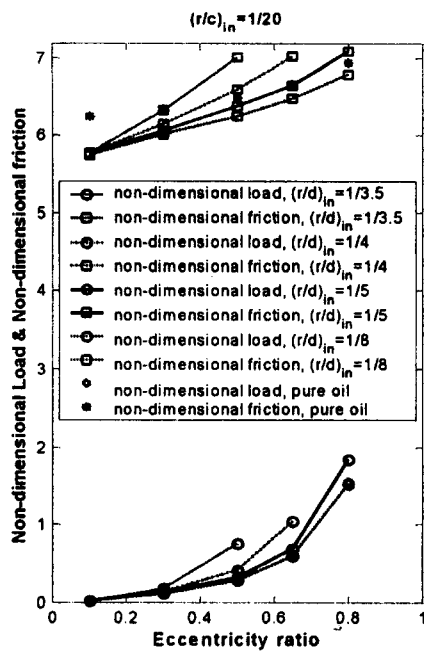
Fig. 3. Non-dimensional load and friction vs. eccentricity ratio at $(r/c)_{in} = 1/20$.
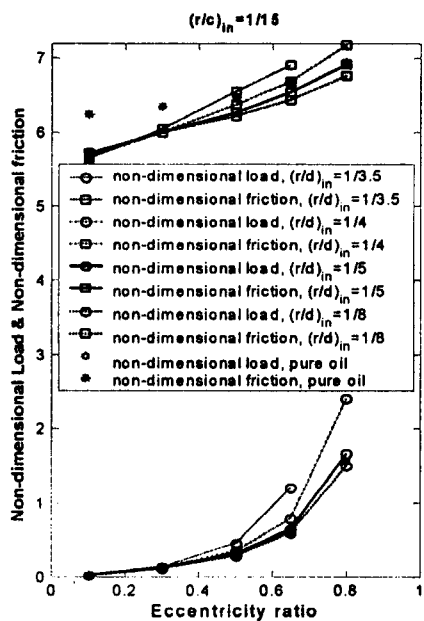

Fig. 4. Non-dimensional load and friction vs. eccentricity ratio at $(r/c)_{in} = 1/15$.
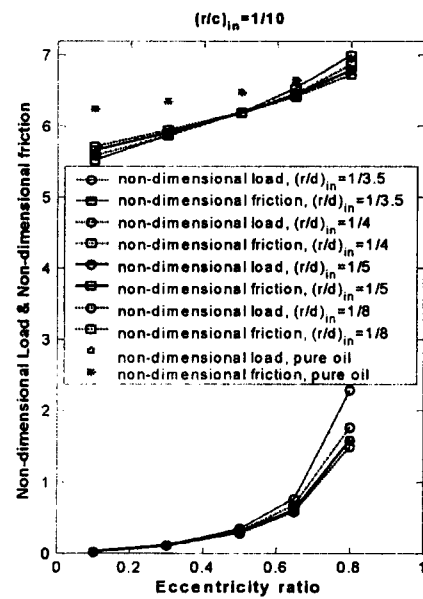

Fig. 5. Non-dimensional load and friction vs. eccentricity ratio at $(r/c)_{in} = 1/10$.

Fig. 6. Non-dimensional load and friction vs. eccentricity ratio at $(r/c)_{in} = 1/7$.

increasing eccentricity ratio. And the higher the aeration level is, the more the non-dimensional load and friction occur. Also, the smaller the air bubble size, the more the non-dimensional load and friction. As the bubble size, $(r/c)_{in}$, increases, the non-dimensional bearing frictions are appeared lower than those under pure oil application, especially at small eccentricity ratios. Meanwhile, the non-dimensional bearing loads under pure oil application are similar to those at aeration level, $(r/d)_{in} = 1/8$ for the most bubble size. If the aeration level decreases, it is appeared that the non-dimensional loads
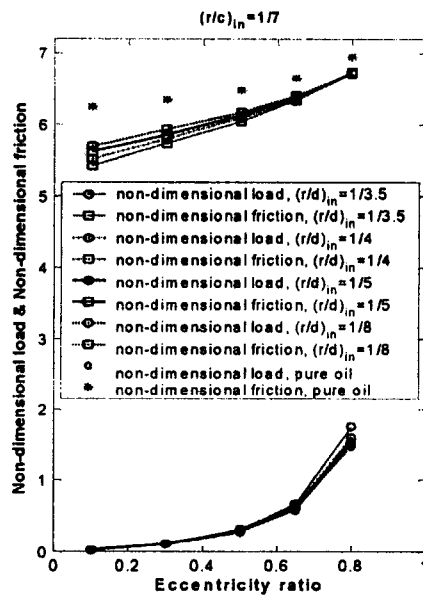
approach to those of pure oil application at all eccentricity ratios without regard to air bubble size.

From the results shown in Fig. 3, it is found that the aerated oil can increase the bearing load of high speed journal bearing by a factor 2.5 with 8% increase of friction force at eccentricity ratio of 0.5, even if the involved aeration levels are not so severe like $(r/d)_{in} = 1/3.5$ and the entrained air bubble sizes are not so small like $(r/c)_{in} = 1/20$. Also, under the conditions of $(r/c)_{in} = 1/20$ and $\varepsilon = 0.5$, the low aeration level like $(r/d)_{in} = 1/8$ can reduce the bearing friction force by 3.5% with keeping the bearing load in the same level as pure oil application.

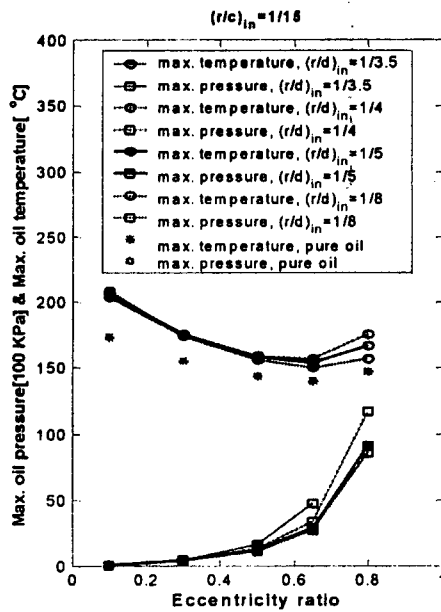From the results shown in Fig. 4, it is also found that the

Fig. 7. Maximum pressure and temperature vs. eccentricity ratio at $(r/c)_{in} = 1/15$.
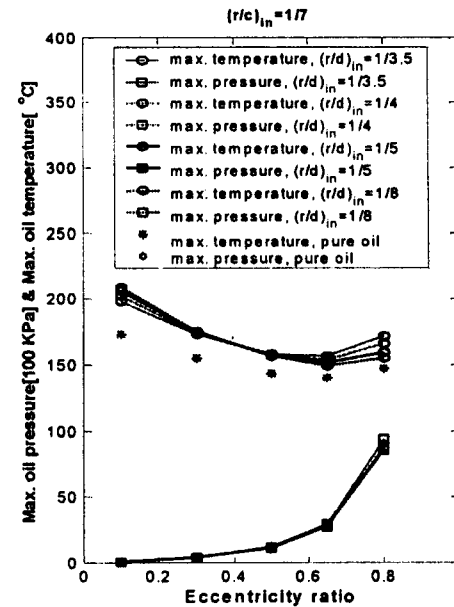

Fig. 8. Maximum pressure and temperature vs. eccentricity ratio at $(r/c)_{in} = 1/7$.

aerated oil can increase the bearing load of high speed journal bearing by a factor two with 5% increase of friction force at eccentricity ratio of 0.65, even if the involved aeration levels are not so severe like $(r/d)_{in} = 1/3.5$ and the entrained air bubble sizes are not so small like $(r/c)_{in} = 1/15$. Also, under the conditions of $(r/c)_{in} = 1/15$ and $\varepsilon = 0.65$, the low aeration level like $(r/d)_{in} = 1/8$ can reduce the bearing friction force by 3% with keeping the bearing load in the same level as pure oil application.

From the results shown in Fig. 5 and Fig.6, if the air bubble size is greater than $(r/c)_{in} = 1/10$, the bearing friction force is appeared as lower than that of pure oil application. Meanwhile, the bearing load increases with increasing aeration level and is appeared as greater than that of pure oil application. As the air bubble size increases, the friction force at the low eccentricity of 0.1 increases with decreasing aeration level. On the other hand, at the high eccentricity of 0.8, the effect of aeration level on the friction force is diminished. This phenomenon can be understood by figuring out the maximum temperature distribution shown in Fig. 7 and Fig. 8.

Under the bearing operating conditions of Table 1, the maximum pressure and temperature are shown in Fig. 7 and Fig. 8 for $(r/c)_{in} = 1/15$ and $1/7$ respectively. It is appeared that the maximum temperature of aerated oil is higher than that of pure oil at any eccentricity ratio. The maximum pressure of pure oil is similar to that of $(r/d)_{in} = 1/5$.

However, with increasing eccentricity ratio, the maximum temperature is changed following a concave curve. As the air bubble size increases, at small eccentricity ratio of $\varepsilon = 0.1$, the maximum temperature increases with decreasing aeration level. But at the moderate range of eccentricity ratio, $\varepsilon = 0.3\sim0.5$, the change of maximum temperature is seen very small with changing the aeration level. Further, at the higher eccentricity ratios, $\varepsilon > 0.65$, the maximum temperature

increases with increasing aeration level. However, the maximum pressure increases all the way with increasing aeration level and eccentricity ratio.

The maximum temperature appears at the bearing downstream in front of the oil supply groove. The bearing clearance at this area increases with increasing eccentricity ratio. The small ratios of eccentricities do not generate sever differences in bearing clearance through whole bearing area. Therefore, for an example, under the condition of a small eccentricity ratio, $\varepsilon = 0.1$, the maximum temperature at the downstream weakly increases with decreasing aeration level as shown Fig. A2 in Appendix. Specially, it can be seen clearly with smaller air bubble size.

Even if, under the condition of small eccentricity ratio, the relatively smaller clearance exists at the bearing downstream compared with the case of higher eccentricity ratio. The change rate of clearance is very small. So, the change of pressure gradient is not so severe in the circumferential direction on oil film. The friction induced by the journal speed on fluid film rather than by the mixed viscosity increase created by the surface tension of air bubble may dominate the temperature distribution of oil film. Therefore, the less the air bubbles exist, the greater the friction occurs and the higher the temperature appears.

But at the moderate range of eccentricity ratio, $\varepsilon = 0.3\sim0.5$, the bearing clearance at the downstream taken place maximum temperature is larger than that at small eccentricity ratio. Therefore, the oil flow may not make sever shear at the downstream. So, the change of the maximum temperature does not clearly appear with regard to the aeration level. At these moderate eccentricities, a little lower bearing clearance can be expected locally at the bearing middle area. But it does not help to increase the temperature notably.

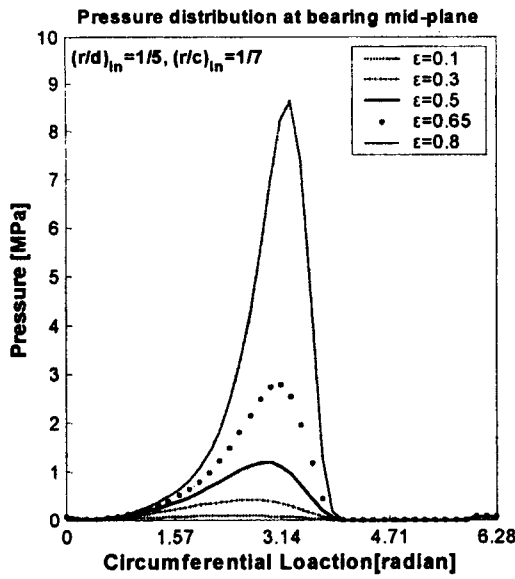However, if the eccentricity ratio increases larger than 0.65,

Fig. 9. Pressure distribution at bearing mid-plane, $(r/d)_{in} = 1/5$ & $(r/c)_{in} = 1/7$.
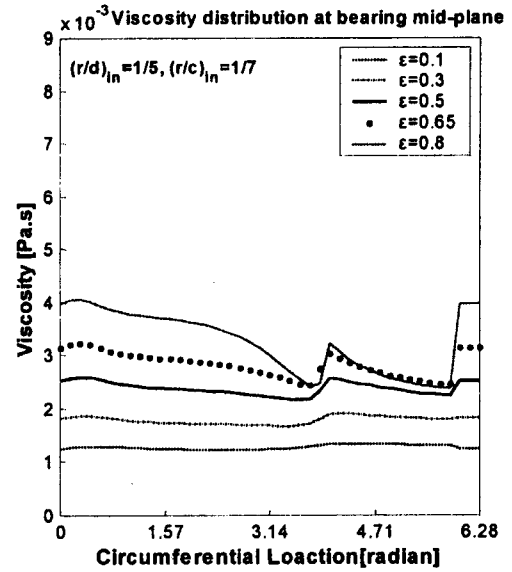

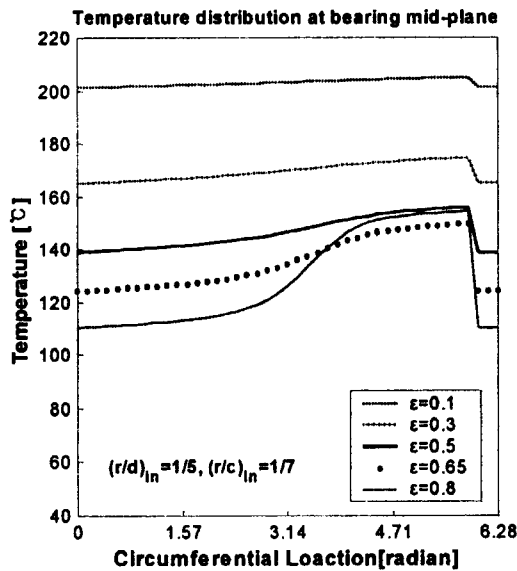Fig. 11. Viscosity distribution at bearing mid-plane, $(r/d)_{in} = 1/5$ & $(r/c)_{in} = 1/7$.

Fig. 10. Temperature distribution at bearing mid-plane, $(r/d)_{in} = 1/5$ & $(r/c)_{in} = 1/7$.

the smaller bearing clearance can be expected locally at the bearing middle area. At this area, the shear of oil film may increase so that the surface tension due to air bubble increase. Therefore, the viscosity and temperature can increase sharply. This brings about the maximum temperature increase at the downstream with increasing aeration level.

Under the relatively bigger air bubble size, $(r/c)_{in} = 1/7$ shown in Fig. 8, at the mid-range of eccentricity ratio below 0.65, the variation of maximum temperature does not appeared with changing aeration level. However, from the eccentricity ratio of 0.65, it is appeared that the maximum temperature increases with increasing aeration level.

In order to understand the results in Fig. 4 and Fig. 7, under the bearing operating conditions of Table 1, the distributions of

pressure, temperature and viscosity at the bearing mid-plane for $(r/c)_{in} = 1/15$ are shown in Fig. A1, Fig. A2 and Fig. A3 for $\varepsilon = 0.1$, and Fig. A4, Fig. A5 and Fig. A6 for $\varepsilon = 0.5$, and Fig. A7, Fig. A8 and Fig. A9 for $\varepsilon = 0.65$. These nine figures are in Appendix.

In order to figure out the results for the case of $(r/d)_{in} = 1/5$ and $(r/c)_{in} = 1/7$ in Fig. 6 and Fig. 8, the distributions of pressure, temperature and viscosity at the bearing mid-plane for $(r/d)_{in} = 1/5$ and $(r/c)_{in} = 1/7$ are shown in Fig. 9, Fig. 10 and Fig. 11 under the bearing operating conditions of Table 1. The pressure distribution increases with increasing eccentricity ratio as usual. The temperature distribution appeared at the bearing downstream increases with decreasing eccentricity ratio. The smaller the eccentricity ratio is, the smaller the clearance appears at the downstream and the more the shear occurs on oil film. Exceptionally, at eccentricity ratio 0.8, the temperature increases sharply from the bearing middle area existing the minimum oil film thickness. Therefore this sudden increase in temperature influences the rise of maximum temperature at the bearing downstream. The viscosity distribution generally increases with increasing eccentricity ratio. Specially, at the high eccentricity ratio, $\varepsilon = 0.8$, the viscosity distribution is appeared with severe fluctuation. The viscosity decreases moderately due to temperature increase along the circumferential direction from the front of the location existing the minimum oil film thickness. Then the viscosity sharply increases due to the high shear. After passing through this area, the viscosity decreases again due to the temperature increase in front of the oil supply groove. At the starting area of oil supply groove, the viscosity increases due to the lower mixing temperature.

Conclusions

1. The non-dimensional load and friction increase with

increasing eccentricity ratio as usual.

2. The higher the aeration level is, the more the non-dimensional load and friction occur. Also, the smaller the air bubble size is, the more the non-dimensional load and friction appear.

3. As the bubble size increases, the bearing frictions are appeared lower than those under pure oil application, especially at small eccentricity ratio.

4. If the aeration level decreases, it is appeared that the bearing loads approach to those of pure oil application at all eccentricity ratios.

5. It is found that the aerated oil can increase the bearing load of high speed journal bearing by a factor two with small increase of friction force at moderate eccentricity ratio, even if the involved aeration levels are not so severe and the entrained air bubble sizes are not so small. Also, the low aeration level can reduce the bearing friction force within small range with keeping the bearing load in the same level as pure oil application.

6. With increasing eccentricity ratio, the maximum temperature is changed following a concave curve. However, the maximum pressure increases all the ways with increasing eccentricity ratio.

Nomenclature

c	=	radial clearance between journal and its bearing (m)
C_p	=	specific heat of lubricant(kJ/kg °C)
d	=	distance between two bubbles (m)
d_{in}	=	distance between two bubbles at inlet condition (m)
$\bar{d}$	=	non-dimensional distance between two bubbles = d/c
$\bar{d}_{in}$	=	non-dimensional distance between two bubbles at inlet condition = d_{in}/c
D	=	bearing diameter (m)
D_m	=	degree of misalignment (the percentage reduction of minimum film thickness at the bearing ends)
e	=	eccentricity(the offset distance between journal and bearing centers)
F	=	friction force
$\bar{F}$	=	non-dimensional friction force = (F/LD) (c/R)/(N)(L/D)
h	=	oil film thickness (m)
$\bar{h}$	=	non-dimensional film thickness = h/c
h_{in}	=	oil film thickness at inlet (m)
$\bar{h}_{in}$	=	non-dimensional film thickness at inlet = h_{in}/c
$H_{bT, sT}$	=	convective heat transfer coefficient at bush and shaft (W/m²°C)
L	=	bearing length (m)
N	=	rotational speed (rpm)
$\bar{p}$	=	mean absolute pressure for turbulent flow (Pa)
$\bar{p}_g$	=	mean gage pressure for turbulent flow (Pa)
$\bar{\underline{p}}$	=	$\bar{p}/(\rho_{oil}RT)$
P	=	non-dimensional mean pressure $(\bar{p}_g(c/R)^2/\mu_0 N)$
$\bar{P}$	=	non-dimensional effective pressure $(H^{3/2}\bar{P}/\bar{\mu}^{1/2})$
P_{in}	=	inlet gage pressure (Pa)
$q_{bT, sT}$	=	turbulent heat transfer to the bush and shaft (W)

Q_{zt}	=	lubricant side leakage (m³/s)
Q_{zt}	=	non-dimensional lubricant side leakage (Q_{zt}/NcR^2)
r	=	bubble radius (m)
r_{in}	=	bubble radius at inlet condition (m)
$\bar{r}$	=	non-dimensional bubble radius = $\dfrac{r}{c}$
$\bar{r}_{in}$	=	non-dimensional bubble radius at inlet condition = r_{in}/c
R	=	journal bearing radius (m)
$\bar{T}$	=	mean temperature for turbulent flow(°C)
T	=	non-dimensional mean temperature

$$= \frac{\rho C_0 (c/R)^2}{2\pi\mu_0 N}(\bar{T} - T_{in})$$

T_{in}	=	inlet oil temperature (°C)
T_b	=	temperature of the bush (°C)
T_s	=	temperature of the shaft (°C)
T_f	=	Fahrenheit temperature (°F)
T_r	=	Rankin temperature (°R)
U	=	speed of journal (m/s)
V	=	air volume fraction
W	=	applied load
$\bar{W}$	=	non-dimensional load parameter

$$= \left(\frac{W}{LD}\left(\frac{c}{R}\right)^2\left(\frac{L}{D}\right)/(\mu_0 N)\right)$$

x,z	=	coordinates of circumferential and axial directions, respectively
$\theta, \bar{z}$	=	non-dimensional coordinates ($\theta = x/R$ $\bar{z} = z/R$)
α	=	viscosity-temperature coefficient(1/ °C)
β	=	vertical misalignment angle (degree)
δ	=	air/oil mass ratio
ε	=	eccentricity ratio = e/c
μ	=	oil viscosity (Pa.s)
μ_0	=	inlet oil viscosity (Pa.s)
μ_{oil}	=	pure oil viscosity (Pa.s)
$\bar{\mu}$	=	μ/μ_{oil}
ρ	=	oil density (kg/m³)
ρ_{oil}	=	pure oil density (kg/m³)
$\bar{\rho}$	=	non-dimensional density = ρ/ρ_{oil}
σ	=	surface tension of air bubble (N/m)
$\bar{\sigma}$	=	$\sigma/(\rho_{oil}RT_c)$
ν	=	oil kinematic viscosity (cSt)
ν_{oil}	=	pure oil kinematic viscosity (cSt)
ϕ	=	misalignment directional angle, i.e., the angle between the plane of the misalignment and the axial plane containing the load vector
φ	=	attitude angle, i.e., angle between the line of centers and the axial plane containing the load vector

References

1. Wilcock, D. F., Turbulence in High Speed Journal Bearing, Trans. of the ASME, Vol. 72, 1950, pp 825-834.

2. Constantinescu, V. N., Theory of Turbulent Lubrication, Proc. Int. Symp. on Lubrication and Wear, University of Houston, 1965, pp 153-213.

3. Ng, C. W. and Pan, C. H. T., A Linearized Turbulent

Lubrication Theory, *Trans. of the ASME, J. of Basic Engineering*, Vol. 87, 1965, pp 675-688.

4. Taylor, C. M., Turbulent Lubrication Theory Applied to Fluid Film Bearing Design, *Proc. Inst. Mech. Engrs.*, Vol. 184, Part 3L, 1969-1970, pp 40-47.

5. Constantinescu, V. N., Basic Relationships in Turbulent Lubrication and Their Extension to Include Thermal Effects, *Trans. of the ASME, J. of Lubrication Technology*, Vol. 95, 1973, pp 147-154.

6. Safar, Z. and Szeri, A. Z., Thermohydrodynamic Lubrication in Laminar and Turbulent Regimes, *Trans. of the ASME, J. of Lubrication Technology*, Vol. 96, 1974, pp 48-57.

7. Szeri, A. Z., *Tribology: Friction, Lubrication and Wear*, Chapter 5, Turbulence, Inertia, and Thermal Effects in Fluid Film Bearings, Hemisphere Publishing Corp., 1980, pp 229-294.

8. Hayward, A. T. J., The viscosity of bubbly Oil, National Engineering Laboratory, Fluids Report No. 99, Glasgow, U. K., 1961.

9. Smith, E. H., The Influence of Surface Tension on Bearings Lubricated With Bubbly Liquids, *Trans. of the ASME, Jour. of Lub. Tech.*, Vol. 102, 1980, pp 91-96.

10. Abdel-Latif, L. A., Peeken, H. and Benner, J., Thermohydrodynamic Analysis of Trust-Bearing With Circular Pads Running on Bubbly Oil (BTHD-Theory), *Trans. of the ASME, Jour. of Trib.*, Vol. 107, 1985, pp 527-537.

11. Chamniprasart, K., Al-Sharif, A., Rajagopal, K. R. and Szeri, A. Z., Lubrication with Binary Mixtures: Bubbly Oil, *Trans.*

of the ASME, Jour. of Trib., Vol. 115, 1993, pp 253-260.

12. Nikolajsen, J. L., Viscosity and Density Models for Aerated Oil in Fluid-Film Bearings, *STLE, Tribology Transactions*, Vol. 42, No. 1, 1999, pp 186-191.

13. Nikolajsen, J. L., The Effect of Aerated Oil on the Load Capacity of Plain Journal Bearing, *STLE, Tribology Transactions*, Vol. 42, No. 1, 1999, pp 58-62.

14. Gazley, C. Jr., Heat-Transfer Characteristics of the Rotational Axial Flow Between Concentric Cylinders, *Trans. of the ASME*, Vol. 80, 1958, pp 79-90.

15. Lin, H. S., Viscosity of Motor Oil, Federal Mogul, Engineering Report, 1981.

16. Holman, J. P., *Heat Transfer*, McGraw-Hill, Inc., 1986, pp 641.

17. Audul-Majeed, G. H. and Al-Soof, N. B. A., Estimation of gas-oil surface tension, *Journal of Petroleum Science and Engineering*, Vol. 27, 2000, pp 197-200.

18. Chun, S. M. and Lalas, D. P., Parametric Study of Inlet Oil Temperature and Pressure for a Half-Circumferential Grooved Journal Bearing, *STLE, Tribology Transaction*, Vol. 35, No. 2, 1992, pp 213-224.

19. Boncompain, R., Fillon, M. and Frene, J., Analysis of Thermal Effects in Hydrodynamic Bearings, *Trans. of the ASME, Jour. of Trib.*, Vol. 108, 1986, pp 219-224.

20. Chun, S. M. and Jang, S., A Parametric Study of Thermal Effects in High Speed Journal Bearing, in *STLE 56th Annual Meeting*, Orlando, Florida, May 20-24, 2001, STLE Presentation No. 01-NP-2.
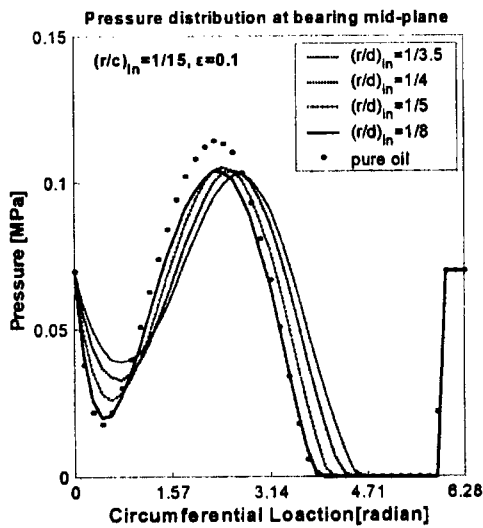
Appendix

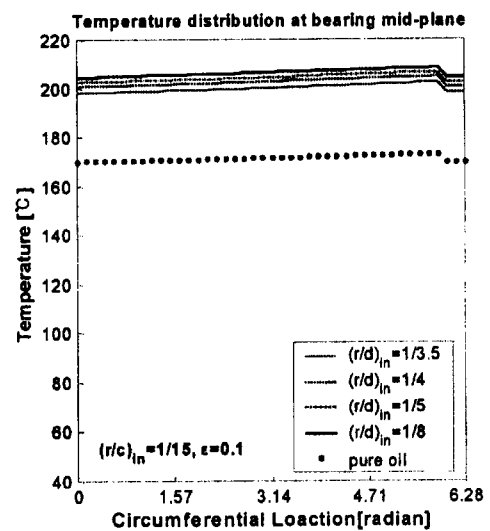Fig. A1. Pressure distribution at bearing mid-plane, $(r/c)_{in}$ = 1/15 & ε = 0.1.

Fig. A2. Temperature distribution at bearing mid-plane, $(r/c)_{in}$ = 1/15 & ε = 0.1.
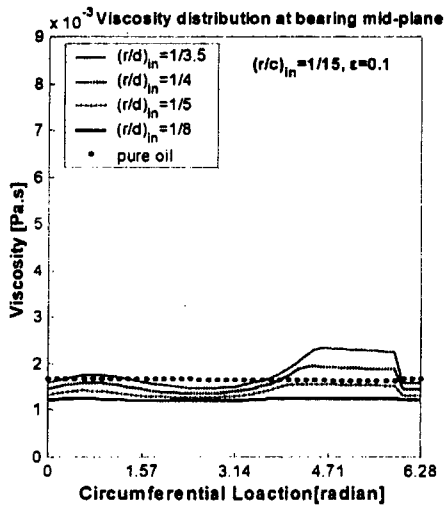
Fig. A3. Viscosity distribution at bearing mid-plane,
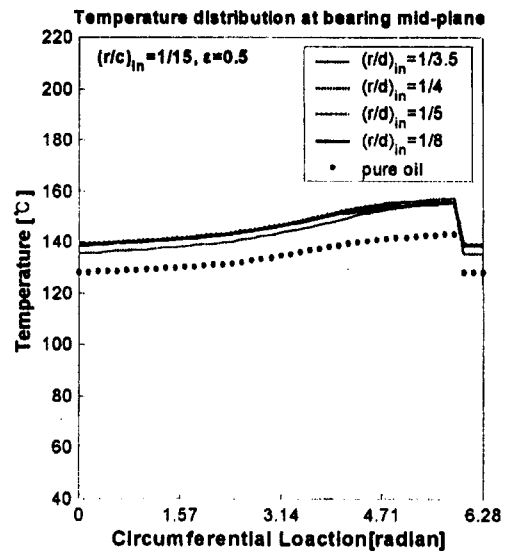$(r/c)_{in}$ = 1/15 & ε = 0.1.

Fig. A4. Pressure distribution at bearing mid-plane,
$(r/c)_{in}$ = 1/15 & ε = 0.5.

Fig. A5. Temperature distribution at bearing mid-plane
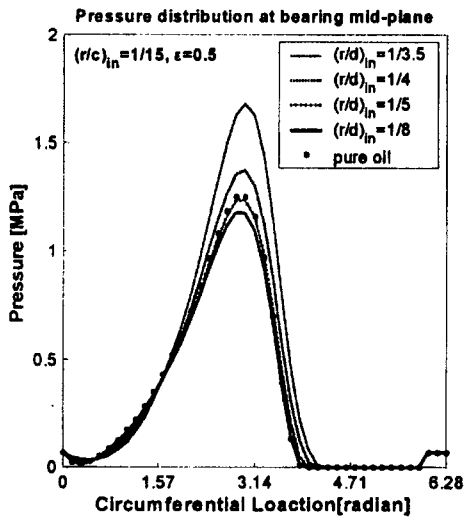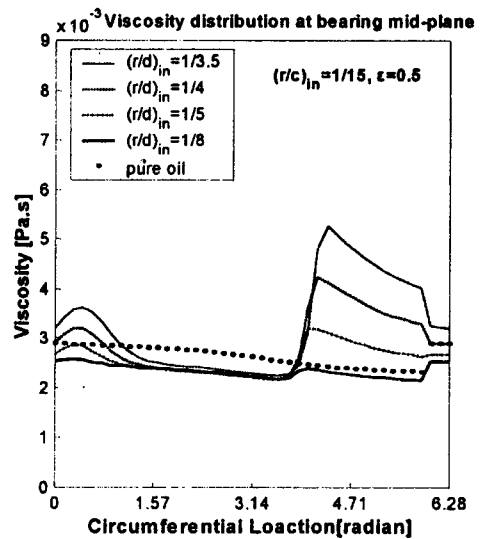$(r/c)_{in}$ = 1/15 & ε = 0.5.

Fig. A6. Viscosity distribution at bearing mid-plane,
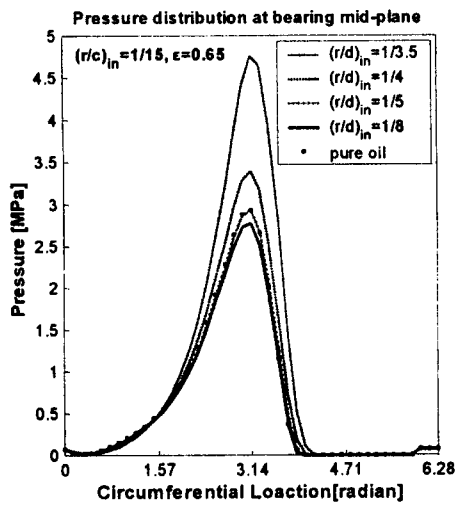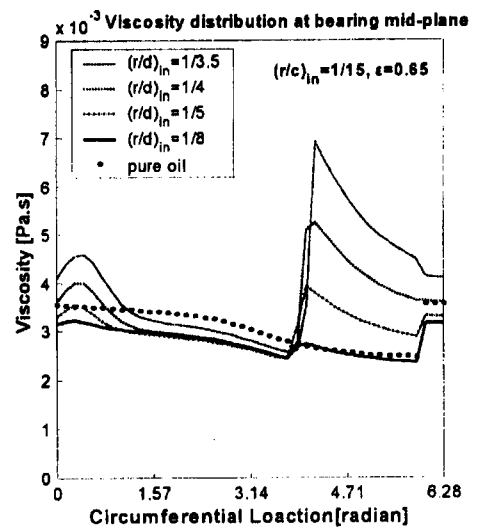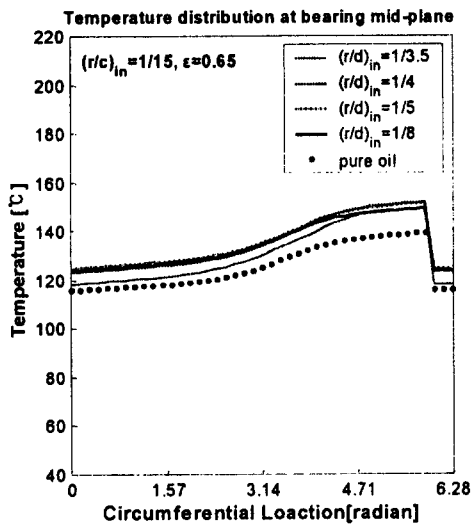$(r/c)_{in}$ = 1/15 & ε= 0.5.

Pressure distribution at bearing mid-plane

Fig. A7. Pressure distribution at bearing mid-plane, $(r/c)_{in}$ = 1/15 & ε= 0.65.

x 10⁻³ Viscosity distribution at bearing mid-plane

Fig. A9. Viscosity distribution at bearing mid-plane, $(r/c)_{in}$ = 1/15 & ε = 0.65.

Temperature distribution at bearing mid-plane

Fig. A8. Pressure distribution at bearing mid-plane, $(r/c)_{in}$ = 1/15 & ε= 0.65.